Journal of Vibration Engineering & Technologies (2023) 11:3293–3305
https://doi.org/10.1007/s42417-022-00749-9

ORIGINAL PAPER

# Investigation of Non-axisymmetric Lamb Wave in an Elastic Plate with Free Boundaries

**Kai Zhou[1] · Yanhong Guan[2] · Quanquan Zhang[2] · Yajing Wang[2] · Xinsheng Xu[2]**

Received: 24 August 2022 / Revised: 8 October 2022 / Accepted: 11 October 2022 / Published online: 26 October 2022


## Abstract

**Purpose** Lamb wave is widely used in damage detection and structural health monitoring of plate-like structures. In the current stage, the propagation of non-axisymmetric circular crested Lamb has not been theoretically solved. Therefore, it is essential to find its exact solutions.

**Methods** The displacement expressions and frequency equations are derived through three-dimensional elastic theory using Helmholtz conversion. Numerical simulations and experiments are conducted on plates for verification of theoretical results.

**Results** Both axisymmetric and non-axisymmetric waves are obtained from the governing equation with free boundary conditions. Lamb wave travels along the radial direction and holds as a standing wave in circumferential and longitudinal directions. The displacement field is expressed with Bessel functions in the radial direction and trigonometric functions in circumferential and longitudinal directions. Two families of Lamb wave modes are generated, which are identified by radial wavenumber and circumferential order. The amplitudes of displacements decrease with the propagation distance increases, and the circumferential distributions of displacements are affected by the circumferential order. Results obtained from simulation and experiment provide good verification for theoretical predictions.

**Conclusions** The analytic solutions are presented in non-axisymmetric problems for circular crested Lamb wave in this paper, which provides a theoretical foundation for further investigation of Lamb wave propagation in plates.

**Keywords** Circular crested Lamb wave · Non-axisymmetric Lamb wave · Frequency equation · Wavenumber

## Introduction

Non-destructive and structural health monitoring systems (SHM) have been widely used in various fields for the ability to increase reliability and safety [1–7]. Lamb wave-based non-destructive and SHM techniques attract increasing attention and have been investigated in many aspects [8–13]. The analytical prediction is a simple and effective method for the propagation of Lamb wave. Characteristics like phase velocity, group velocity and dispersion can be obtained through the theoretical method [14], which play important roles in the application of different situations [15–18] of SHM.

The propagation of Lamb wave in plate-like structures has been discussed since the end of the nineteenth century, Rayleigh [19] and Lamb [20] first established the frequency equations, i.e., the well-known Rayleigh-Lamb equation. The plane Lamb wave is considered with the plane strain assumption in their derivation. As a consequence, the wavefront is assumed as an infinite plane normal to the propagation direction. Such results of the Lamb wave have been extended to anisotropic and viscoelastic media in the following investigation [21–23].

The theory of wave propagation in media including arbitrary amounts of parallel plates with different materials and thicknesses was proposed by Thomson in 1950 [24]. The stress of each layer is derived from the coupling conditions at interfaces and free boundary at the top as well as the bottom surface. The matrix method is adopted to produce frequency equations in a form suitable for understanding and

✉ Xinsheng Xu
xsxu@dlut.edu.cn

[1] School of Urban Construction, Yangtze University, Jingzhou 434023, China

[2] State Key Laboratory of Structure Analysis of Industrial Equipment, Department of Engineering Mechanics, Dalian University of Technology, Dalian 116024, China

computing. Following Thomson's work, some researchers investigated the Lamb wave in multilayered media [25–27].

The above research work is based on the assumption of the plane wavefront, in which the size of excitation loading must be infinite. The reason is that the vibration normal to the propagation direction (but not through the plate thickness) is neglected in the plane wavefront assumption [28]. For this reason, the plane wave model (with plane wavefront assumption) is not exact in practice. In fact, almost all Lamb waves that existed in plates are circular crested waves [29, 30] whose wavefront travel as a circular from the origin. Goodman derived the circular crested Lamb wave in isotropic plates excited by axisymmetric loading [31]. The axisymmetric case is considered which implies with the same propagation distance, the vibration is constant along different propagation directions. Similarities and discrepancies between circular crested Lamb wave and plane Lamb wave are revealed. The frequency equation and across thickness displacements are proved to be the same as that of plane Lamb wave in the same plates [32, 33].

Besides the axisymmetric case of circular crested Lamb wave, the non-axisymmetric solutions are also of great significance for most of the excitation in practice is not axisymmetric. In this work, the complete solutions of both axisymmetric and non-axisymmetric Lamb wave in isotropic plates are derived and presented with the cylindrical coordinate system. The solution of the circular crested Lamb wave based on the governing equation is demonstrated in detail. The Helmholtz conversion concerning displacements is adopted for clarity of presentation. The displacement expressions and frequency equations are obtained by satisfying free boundary conditions at the surfaces of the plate, and characteristics of circular crested Lamb wave displacements are discussed. Simulations as well as experiments are conducted on plates to verify the results predicted by theoretical formulations.

## The Fundamental Problem

Consider an isotropic plate in Fig. 1. A cylindrical coordinate system $(r, \theta, z)$ is adopted to describe the field of wave motion. The plate is infinite in the $r$–$\theta$ plane and has a finite thickness $2h$ in the longitudinal $(z)$ direction. The upper and lower surfaces of the plate are located at $z=h$ and $z=-h$, respectively.

The time-harmonic waves are considered by means of a time dependence factor $e^{-i\omega t}$, which is omitted for brevity in the following derivation, where $\omega=2\pi f$ denotes the angular frequency, and $f$ denotes the frequency. Based on the continuity conditions $g(\theta_0)=g(\theta_0+2\pi)$ for an arbitrary field variable $g$ (displacement, strain, stress et al.) with an arbitrary $\theta_0$, the angle dependence factor can be

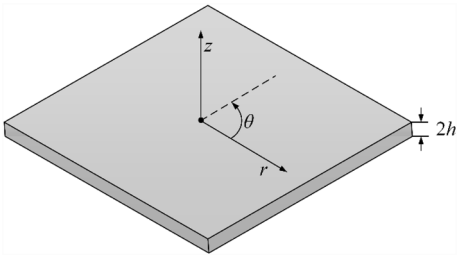


**Fig. 1** An isotropic plate in a cylindrical coordinate system

described as $e^{in\theta}$ $(n=0, 1, 2, \ldots)$. The governing equations are expressed in an invariant form

$$(\lambda+\mu)\nabla\nabla\cdot\boldsymbol{u}+\mu\nabla^2\boldsymbol{u}=\rho\frac{\partial^2\boldsymbol{u}}{\partial t^2}, \tag{1}$$

where $\lambda$ and $\mu$ are Lame's constants, $\rho$ is the mass density, $\boldsymbol{u}=(u, v, w)^{\mathrm{T}}$ is the displacement vector in $(r, \theta, z)$ direction. Equation (1) includes three partial differential equations with difficult to solve. A convenient method of dealing with this problem is through Helmholtz conversion [34]. The displacement vector is expressed in terms of a dilatational scalar potential $\varphi$ and an equivoluminal vector potential $\boldsymbol{\psi}$

$$\boldsymbol{u}=\nabla\varphi+\nabla\times\boldsymbol{\psi}, \tag{2}$$

with

$$\nabla\cdot\boldsymbol{\psi}=0. \tag{3}$$

In a cylindrical coordinate system, the displacement can be expressed as

$$\begin{cases} u=\frac{\partial\varphi}{\partial r}+\frac{1}{r}\frac{\partial\psi_3}{\partial\theta}-\frac{\partial\psi_2}{\partial z} \\ v=\frac{1}{r}\frac{\partial\varphi}{\partial\theta}+\frac{\partial\psi_1}{\partial z}-\frac{\partial\psi_3}{\partial r} \\ w=\frac{\partial\varphi}{\partial z}+\frac{\partial\psi_2}{\partial r}+\frac{1}{r}\psi_2-\frac{1}{r}\frac{\partial\psi_1}{\partial\theta} \end{cases} \tag{4}$$

where $\boldsymbol{\psi}=(\psi_1, \psi_2, \psi_3)^{\mathrm{T}}$. And the potentials $\varphi$ and $\boldsymbol{\psi}$ satisfy the wave equations

$$\begin{aligned} c_l^2\nabla^2\varphi&=\frac{\partial^2\varphi}{\partial t^2} \\ c_s^2\nabla^2\boldsymbol{\psi}&=\frac{\partial^2\boldsymbol{\psi}}{\partial t^2}, \end{aligned} \tag{5}$$

where

$$\begin{aligned} c_l^2&=(\lambda+2\mu)/\rho \\ c_s^2&=\mu/\rho. \end{aligned} \tag{6}$$

The scalar potential $\varphi$ describes a longitudinal wave with the velocity $c_l$, while the vector potential $\boldsymbol{\psi}$ describes a shear wave with the velocity $c_s$. Equation (5) can be rewritten as

$$\begin{cases} c_l^2\left(\frac{\partial^2}{\partial r^2}+\frac{1}{r}\frac{\partial}{\partial r}-\frac{n^2}{r^2}+\frac{\partial^2}{\partial z^2}\right)\varphi-\frac{\partial^2\varphi}{\partial t^2}=0 \\ c_s^2\left(\frac{\partial^2}{\partial r^2}+\frac{1}{r}\frac{\partial}{\partial r}-\frac{n^2}{r^2}+\frac{\partial^2}{\partial z^2}-\frac{1}{r^2}\right)\psi_1-c_s^2\frac{2in}{r^2}\psi_2-\frac{\partial^2\psi_1}{\partial t^2}=0 \\ c_s^2\left(\frac{\partial^2}{\partial r^2}+\frac{1}{r}\frac{\partial}{\partial r}-\frac{n^2}{r^2}+\frac{\partial^2}{\partial z^2}-\frac{1}{r^2}\right)\psi_2+c_s^2\frac{2in}{r^2}\psi_1-\frac{\partial^2\psi_2}{\partial t^2}=0 \\ c_s^2\left(\frac{\partial^2}{\partial r^2}+\frac{1}{r}\frac{\partial}{\partial r}-\frac{n^2}{r^2}+\frac{\partial^2}{\partial z^2}\right)\psi_3-\frac{\partial^2\psi_3}{\partial t^2}=0 \end{cases} \tag{7}$$

It should be noticed that the second and third equations in Eq. (7) include both the potentials $\psi_1$ and $\psi_2$. Therefore, we introduce the transformation of variables

$$\begin{cases} \tilde{\psi}_1=\psi_1+i\psi_2 \\ \tilde{\psi}_2=\psi_1-i\psi_2 \end{cases}. \tag{8}$$

The corresponding inverse transformation is

$$\begin{cases} \psi_1=\frac{1}{2}\left(\tilde{\psi}_1+\tilde{\psi}_2\right) \\ \psi_2=-\frac{1}{2}i\left(\tilde{\psi}_1-\tilde{\psi}_2\right) \end{cases}. \tag{9}$$

Equation (7) can be rewritten as

$$\begin{cases} c_l^2\left(\frac{\partial^2}{\partial r^2}+\frac{1}{r}\frac{\partial}{\partial r}-\frac{n^2}{r^2}\right)\varphi+c_l^2\frac{\partial^2}{\partial z^2}\varphi+\omega^2\varphi=0 \\ c_s^2\left[\frac{\partial^2}{\partial r^2}+\frac{1}{r}\frac{\partial}{\partial r}-\frac{(n+1)^2}{r^2}\right]\tilde{\psi}_1+c_s^2\frac{\partial^2}{\partial z^2}\tilde{\psi}_1+\omega^2\tilde{\psi}_1=0 \\ c_s^2\left[\frac{\partial^2}{\partial r^2}+\frac{1}{r}\frac{\partial}{\partial r}-\frac{(n-1)^2}{r^2}\right]\tilde{\psi}_2+c_s^2\frac{\partial^2}{\partial z^2}\tilde{\psi}_2+\omega^2\tilde{\psi}_2=0 \\ c_s^2\left(\frac{\partial^2}{\partial r^2}+\frac{1}{r}\frac{\partial}{\partial r}-\frac{n^2}{r^2}\right)\psi_3+c_s^2\frac{\partial^2}{\partial z^2}\psi_3+\omega^2\psi_3=0 \end{cases}. \tag{10}$$

Equation (10) includes four partial differential equations, each of which only contains one unknown function. The part concerning variable $r$ in Eq. (10) is the Bessel equation, the solution of which can be expressed by the Bessel function.

## The Fundamental Solutions

The solution of Eq. (10) can be expressed as

$$\begin{cases} \varphi(r,\theta,z,t)=J_n(kr)f_0(z)e^{in\theta} \\ \tilde{\psi}_1(r,\theta,z,t)=J_{n+1}(kr)f_1(z)e^{in\theta} \\ \tilde{\psi}_2(r,\theta,z,t)=J_{n-1}(kr)f_2(z)e^{in\theta} \\ \psi_3(r,\theta,z,t)=J_n(kr)f_3(z)e^{in\theta} \end{cases}, \tag{11}$$

where $J_n$ is the Bessel function of order $n$ satisfying

$$\left[\frac{\partial}{\partial r^2}+\frac{1}{r}\frac{\partial}{\partial r}+\left(k^2-\frac{n^2}{r^2}\right)\right]J_n(kr)=0. \tag{12}$$

Substitution of Eq. (11) into Eq. (10) yields

$$\begin{cases} c_l^2f_0''(z)+\left(\omega^2-c_l^2k^2\right)f_0(z)=0 \\ c_s^2f_1''(z)+\left(\omega^2-c_s^2k^2\right)f_1(z)=0 \\ c_s^2f_2''(z)+\left(\omega^2-c_s^2k^2\right)f_2(z)=0 \\ c_s^2f_3''(z)+\left(\omega^2-c_s^2k^2\right)f_3(z)=0 \end{cases} \tag{13}$$

The general solution of Eq. (13) can be written as

$$\begin{cases} f_0(z)=A_1\cos\alpha z+A_2\sin\alpha z \\ f_1(z)=A_3\cos\beta z+A_4\sin\beta z \\ f_2(z)=A_5\cos\beta z+A_6\sin\beta z \\ f_3(z)=A_7\cos\beta z+A_8\sin\beta z \end{cases} \tag{14}$$

where $A_i$ ($i=1, 2, \ldots, 8$) is arbitrary coefficients, and

$$\alpha=\sqrt{\frac{\omega^2}{c_l^2}-k^2},\quad \beta=\sqrt{\frac{\omega^2}{c_s^2}-k^2} \tag{15}$$

The coefficients in Eq. (14) are dependently caused by Eq. (3) which can be expanded as

$$\frac{1}{r}\frac{\partial}{\partial r}(r\psi_1)+\frac{in}{r}\psi_2+\frac{\partial\psi_3}{\partial z}=0 \tag{16}$$

Considering the transformation in Eq. (9) and using the properties of Bessel functions, the relation between different coefficients can be obtained

$$\begin{cases} A_7=\frac{k}{2\beta}A_4-\frac{k}{2\beta}A_6 \\ A_8=-\frac{k}{2\beta}A_3+\frac{k}{2\beta}A_5 \end{cases} \tag{17}$$

Substitution of Eq. (9) into Eq. (11) gives

$$\begin{cases} \varphi(r,\theta,z,t)=J_n(kr)f_0(z)e^{in\theta} \\ \psi_1(r,\theta,z,t)=\frac{1}{2}\left[J_{n+1}(kr)f_1(z)+J_{n-1}(kr)f_2(z)\right]e^{in\theta} \\ \psi_2(r,\theta,z,t)=-\frac{1}{2}i\left[J_{n+1}(kr)f_1(z)-J_{n-1}(kr)f_2(z)\right]e^{in\theta} \\ \psi_3(r,\theta,z,t)=J_n(kr)f_3(z)e^{in\theta} \end{cases}. \tag{18}$$

The displacement in Eq. (4) can be expressed as

$$
\begin{aligned}
u &= \frac{\partial \varphi}{\partial r} + \frac{in}{r}\psi_3 - \frac{\partial \psi_2}{\partial z} \\
&= \left\{ kJ_n'(kr)f_0(z) + \frac{in}{r}J_n(kr)f_3(z) + \frac{1}{2}i\left[J_{n+1}(kr)f_1'(z) - J_{n-1}(kr)f_2'(z)\right] \right\} e^{in\theta} \\
v &= \frac{in}{r}\varphi + \frac{\partial \psi_1}{\partial z} - \frac{\partial \psi_3}{\partial r} \\
&= \left\{ \frac{in}{r}J_n(kr)f_0(z) + \frac{1}{2}\left[J_{n+1}(kr)f_1'(z) + J_{n-1}(kr)f_2'(z)\right] - kJ_n'(kr)f_3(z) \right\} e^{in\theta} \\
w &= \frac{\partial \varphi}{\partial z} + \frac{\partial \psi_2}{\partial r} + \frac{1}{r}\psi_2 - \frac{in}{r}\psi_1 \\
&= e^{in\theta}\left\{ J_n(kr)f_0'(z) - \frac{1}{2}ik\left[J_{n+1}'(kr)f_1(z) - J_{n-1}'(kr)f_2(z)\right] \right. \\
&\quad \left. -\frac{1}{2r}i\left[J_{n+1}(kr)f_1(z) - J_{n-1}(kr)f_2(z)\right] - \frac{in}{2r}\left[J_{n+1}(kr)f_1(z) + J_{n-1}(kr)f_2(z)\right] \right\}.
\end{aligned} \tag{19}
$$

Taking advantage of the properties existing in Bessel functions

$$
\begin{cases} J_n'(kr) = \frac{1}{2}\left[J_{n-1}(kr) - J_{n+1}(kr)\right] \\ \frac{2n}{x}J_n(kr) = J_{n-1}(kr) + J_{n+1}(kr) \end{cases}, \quad n = 0, \pm 1, \pm 2, \ldots, \tag{20}
$$

the displacement can be expressed as

$$
\begin{aligned}
u &= \left\{ J_{n-1}(kr)\left[B_1\cos\alpha z + B_2\sin\alpha z + iB_6\cos\beta z + iB_5\sin\beta z\right] \right. \\
&\quad \left. + J_{n+1}(kr)\left[-B_1\cos\alpha z - B_2\sin\alpha z + iB_4\cos\beta z + iB_3\sin\beta z\right] \right\} e^{in\theta} \\
v &= \left\{ J_{n+1}(kr)\left[iB_1\cos\alpha z + iB_2\sin\alpha z + B_3\sin\beta z + B_4\cos\beta z\right] \right. \\
&\quad \left. + J_{n-1}(kr)\left[iB_1\cos\alpha z + iB_2\sin\alpha z - B_5\sin\beta z - B_6\cos\beta z\right] \right\} e^{in\theta} \\
w &= J_n(kr)\left\{ \alpha\left(-A_1\sin\alpha z + A_2\cos\alpha z\right) - \frac{k}{2}i\left[\left(A_3 + A_5\right)\cos\beta z + \left(A_4 + A_6\right)\sin\beta z\right] \right\} e^{in\theta},
\end{aligned} \tag{21}
$$

where

$$
\begin{aligned}
&B_1 = \frac{k}{2}A_1, \quad B_2 = \frac{k}{2}A_2, \\
&B_3 = -\frac{k^2}{4\beta}A_3 + \frac{k^2}{4\beta}A_5 - \frac{\beta}{2}A_3, \quad B_4 = \frac{k^2}{4\beta}A_4 - \frac{k^2}{4\beta}A_6 + \frac{\beta}{2}A_4 \\
&B_5 = -\frac{k^2}{4\beta}A_3 + \frac{k^2}{4\beta}A_5 + \frac{\beta}{2}A_5, \quad B_6 = \frac{k^2}{4\beta}A_4 - \frac{k^2}{4\beta}A_6 - \frac{\beta}{2}A_6.
\end{aligned} \tag{22}
$$

## Free Boundary Conditions

The expression of stresses can be derived from the stress and displacement relations

$$
\begin{cases} \sigma_{rz} = \mu\left(\frac{\partial u}{\partial z} + \frac{\partial w}{\partial r}\right) \\ \sigma_{\theta z} = \mu\left(\frac{\partial v}{\partial z} + \frac{1}{r}\frac{\partial w}{\partial \theta}\right) \\ \sigma_{zz} = \lambda\left(\frac{\partial u}{\partial r} + \frac{u}{r} + \frac{1}{r}\frac{\partial v}{\partial \theta}\right) + (\lambda + 2\mu)\frac{\partial w}{\partial z} \end{cases}, \tag{23}
$$

where $\sigma$ represents the stress. The stresses can be described as

$$
\begin{aligned}
\sigma_{rz} &= \mu\left\{ J_{n+1}(kr)\left[C_1\sin\alpha z - C_2\cos\alpha z + iC_6\sin\beta z + iC_5\cos\beta z\right] \right. \\
&\quad \left. + J_{n-1}(kr)\left[-C_1\sin\alpha z + C_2\cos\alpha z + iC_4\sin\beta z + iC_3\cos\beta z\right] \right\} e^{in\theta} \\
\sigma_{\theta z} &= \mu\left\{ J_{n+1}(kr)\left[-iC_1\sin\alpha z + iC_2\cos\alpha z + C_6\sin\beta z + C_5\cos\beta z\right] \right. \\
&\quad \left. + J_{n-1}(kr)\left[-iC_1\sin\alpha z + iC_2\cos\alpha z - C_4\sin\beta z - C_3\cos\beta z\right] \right\} e^{in\theta} \\
\sigma_{zz} &= J_n(kr)\left[-\gamma A_2\sin\alpha z + i\chi\left(A_3 + A_5\right)\sin\beta z \right. \\
&\quad \left. -\gamma A_1\cos\alpha z - i\chi\left(A_4 + A_6\right)\cos\beta z\right] e^{in\theta},
\end{aligned} \tag{24}
$$

where

$$
\begin{aligned}
&C_1 = \alpha k A_1, \quad C_2 = \alpha k A_2, \\
&C_3 = -\frac{k^2}{2}A_3 + \frac{\beta^2}{2}A_5, \quad C_4 = -\frac{k^2}{2}A_4 + \frac{\beta^2}{2}A_6 \\
&C_5 = -\frac{\beta^2}{2}A_3 + \frac{k^2}{2}A_5, \quad C_6 = -\frac{\beta^2}{2}A_4 + \frac{k^2}{2}A_6,
\end{aligned} \tag{25}
$$

and

$$
\gamma = \lambda k^2 + (\lambda + 2\mu)\alpha^2, \quad \chi = \mu\beta k. \tag{26}
$$

It should be remarked that the stress components $\sigma_{rz}$ and $\sigma_{\theta z}$ include two parts described by different orders of Bessel

functions $J_{n+1}(kr)$ and $J_{n-1}(kr)$, which affect the analysis and processing of boundary conditions. To avoid this problem, the conversion

$$\begin{aligned}\sigma_1 &= \frac{i\sigma_{rz}+\sigma_{\theta z}}{2}\\ &= J_{n-1}(kr)\left[-iC_1\sin\alpha z + iC_2\cos\alpha z - C_4\sin\beta z - C_3\cos\beta z\right]e^{in\theta}\\ \sigma_2 &= \frac{i\sigma_{rz}-\sigma_{\theta z}}{2}\\ &= J_{n+1}(kr)\left[iC_1\sin\alpha z - iC_2\cos\alpha z - C_6\sin\beta z - C_5\cos\beta z\right]e^{in\theta}\end{aligned} \tag{27}$$

is introduced. The boundary conditions of free motion at the surfaces of the plate are

$$\sigma_{rz}\big|_{z=\pm h} = \sigma_{\theta z}\big|_{z=\pm h} = \sigma_{zz}\big|_{z=\pm h} = 0. \tag{28}$$

The corresponding and equivalent conditions of Eq. (28) are

$$\sigma_1\big|_{z=\pm h} = \sigma_2\big|_{z=\pm h} = \sigma_{zz}\big|_{z=\pm h} = 0. \tag{29}$$

Substitution of Eq. (29) into Eq. (27) yields

$$\begin{aligned}&\mp iC_1\sin\alpha h + iC_2\cos\alpha h \mp C_4\sin\beta h - C_3\cos\beta h = 0\\ &\pm iC_1\sin\alpha h - iC_2\cos\alpha h \mp C_6\sin\beta h - C_5\cos\beta h = 0\\ &\mp\gamma A_2\sin\alpha h \pm i\chi\left(A_3+A_5\right)\sin\beta h - \gamma A_1\cos\alpha h - i\chi\left(A_4+A_6\right)\cos\beta h = 0\end{aligned} \tag{30}$$

Equation (30) can be written as its equivalent expression

$$\begin{cases} 2\alpha kiA_2\cos\alpha h + \left(k^2A_3 - \beta^2A_5\right)\cos\beta h = 0\\ -2\alpha kiA_1\sin\alpha h + \left(k^2A_4 - \beta^2A_6\right)\sin\beta h = 0\\ -2\alpha kiA_2\cos\alpha h + \left(\beta^2A_3 - k^2A_5\right)\cos\beta h = 0\\ 2\alpha kiA_1\sin\alpha h + \left(\beta^2A_4 - k^2A_6\right)\sin\beta h = 0\\ \left(k^2-\beta^2\right)iA_1\cos\alpha h + \beta k\left(A_4+A_6\right)\cos\beta h = 0\\ \left(\beta^2-k^2\right)iA_2\sin\alpha h + \beta k\left(A_3+A_5\right)\sin\beta h = 0\end{cases}. \tag{31}$$

## Frequency Equations

Equation (31) can be divided into two independent parts as

$$\begin{cases} -2\alpha kiA_1\sin\alpha h + \left(k^2A_4 - \beta^2A_6\right)\sin\beta h = 0\\ 2\alpha kiA_1\sin\alpha h + \left(\beta^2A_4 - k^2A_6\right)\sin\beta h = 0\\ \left(k^2-\beta^2\right)iA_1\cos\alpha h + \beta k\left(A_4+A_6\right)\cos\beta h = 0\end{cases} \tag{32}$$

for symmetric (S) motion, and

$$\begin{cases} 2\alpha kiA_2\cos\alpha h + \left(k^2A_3 - \beta^2A_5\right)\cos\beta h = 0\\ -2\alpha kiA_2\cos\alpha h + \left(\beta^2A_3 - k^2A_5\right)\cos\beta h = 0\\ \left(\beta^2-k^2\right)iA_2\sin\alpha h + \beta k\left(A_3+A_5\right)\sin\beta h = 0\end{cases} \tag{33}$$

for anti-symmetric (A) motion. The frequency equations of both S motion and A motion can be derived from Eqs. (32) and (33) with the requirement of a nontrivial solution for each set of equations as

$$\sin\beta h\begin{vmatrix} -2\alpha k\sin\alpha h & k^2\sin\beta h & -\beta^2\sin\beta h\\ 0 & 1 & -1\\ \left(k^2-\beta^2\right)\cos\alpha h & \beta k\cos\beta h & \beta k\cos\beta h\end{vmatrix} = 0 \tag{34}$$

for S motion, and

$$\cos\beta h\begin{vmatrix} 2\alpha k\cos\alpha h & k^2\cos\beta h & -\beta^2\cos\beta h\\ 0 & 1 & -1\\ \left(\beta^2-k^2\right)\sin\alpha h & \beta k\sin\beta h & \beta k\sin\beta h\end{vmatrix} = 0 \tag{35}$$

for A motion. Both Eqs. (34) and (35) include shear horizontal (SH) wave and Lamb wave. For Lamb wave, frequency equations are expressed as

$$\frac{\tan\beta h}{\tan\alpha h} = -\left[\frac{4\alpha\beta k^2}{\left(\beta^2-k^2\right)^2}\right]^{\pm1}, \tag{36}$$

where + and − describe S motion and A motion, respectively. The frequency equations of circular crested Lamb wave are the same as those of plane Lamb wave [20, 35], and the frequency-dependent wavenumber $k$ can be calculated from the corresponding frequency equation. The transcendental frequency equations provide an infinite number of solutions, leading to infinite series of S modes as well as A modes. The S modes are described as S($m$, $n$), and the A modes are described as A($m$, $n$), where $m$ ($m$=0, 1, 2, …) indicates the $m$th solution of the corresponding frequency equation ($k_m$) and $n$ ($n$=0, 1, 2, …) indicates the circumferential order.

## The Displacement Expressions

The frequency equations have been divided into two parts: S wave and A wave. The two kinds of waves are discussed separately. For S motion, Eq. (32) can be written as

$$\begin{pmatrix} -2\alpha k\sin\alpha h & k^2\sin\beta h & -\beta^2\sin\beta h\\ 2\alpha k\sin\alpha h & \beta^2\sin\beta h & -k^2\sin\beta h\\ \left(k^2-\beta^2\right)\cos\alpha h & \beta k\cos\beta h & \beta k\cos\beta h\end{pmatrix}\begin{pmatrix} iA_1\\ A_4\\ A_6\end{pmatrix} = \begin{pmatrix} 0\\ 0\\ 0\end{pmatrix}. \tag{37}$$

A fundamental solution of Eq. (37) is

$$\begin{cases} A_1 = 2i\beta k\cos\beta h\\ A_4 = \left(k^2-\beta^2\right)\cos\alpha h\\ A_6 = \left(k^2-\beta^2\right)\cos\alpha h\end{cases}. \tag{38}$$

The displacements of this case can be obtained by substituting Eq. (38) into displacement expression in Eq. (21)

$$\begin{aligned} u &= \frac{1}{2}\left[J_{n+1}(kr) - J_{n-1}(kr)\right]\left[-2\beta k^2 \cos\beta h \cos\alpha z + \beta\left(k^2-\beta^2\right)\cos\alpha h \cos\beta z\right]e^{in\theta} \\ v &= \frac{1}{2i}\left[J_{n+1}(kr) + J_{n-1}(kr)\right]\left[-2\beta k^2 \cos\beta h \cos\alpha z + \beta\left(k^2-\beta^2\right)\cos\alpha h \cos\beta z\right]e^{in\theta} \\ w &= J_n(kr)\left[-2\alpha\beta k \cos\beta h \sin\alpha z - k\left(k^2-\beta^2\right)\cos\alpha h \sin\beta z\right]e^{in\theta}. \end{aligned} \tag{39}$$

For A motion, Eq. (33) can be written as

$$\begin{pmatrix} 2\alpha k\cos\alpha h & k^2\cos\beta h & -\beta^2\cos\beta h \\ -2\alpha k\cos\alpha h & \beta^2\cos\beta h & -k^2\cos\beta h \\ \left(\beta^2-k^2\right)\sin\alpha h & \beta k\sin\beta h & \beta k\sin\beta h \end{pmatrix}\begin{pmatrix} iA_2 \\ A_3 \\ A_5 \end{pmatrix} = \begin{pmatrix} 0 \\ 0 \\ 0 \end{pmatrix}. \tag{40}$$

A fundamental solution of Eq. (40) is

$$\begin{cases} A_2 = 2i\beta k\sin\beta h \\ A_3 = \left(\beta^2-k^2\right)\sin\alpha h \\ A_5 = \left(\beta^2-k^2\right)\sin\alpha h \end{cases}. \tag{41}$$

The displacements of this case are derived by substituting the coefficients into displacement expressions

$$\begin{aligned} u &= \frac{1}{2}\left[J_{n+1}(kr) - J_{n-1}(kr)\right]\left[-2\beta k^2 \sin\beta h \sin\alpha z + \beta\left(k^2-\beta^2\right)\sin\alpha h \sin\beta z\right]e^{in\theta} \\ v &= \frac{1}{2i}\left[J_{n+1}(kr) + J_{n-1}(kr)\right]\left[-2\beta k^2 \sin\beta h \sin\alpha z + \beta\left(k^2-\beta^2\right)\sin\alpha h \sin\beta z\right]e^{in\theta} \\ w &= J_n(kr)\left[2\alpha\beta k \sin\beta h \cos\alpha z + k\left(k^2-\beta^2\right)\sin\alpha h \cos\beta z\right]e^{in\theta}. \end{aligned} \tag{42}$$

The displacement field of circular crested Lamb wave has been exactly solved by using a theoretical method. Lamb wave travels along the radial direction from the origin and holds as a standing wave in circumferential and longitudinal directions. Two cases of solution are obtained for one S case as well as one A case with respect to the $z$-axis.

## Results and Discussions

The displacements of Lamb wave can be described as

$$\boldsymbol{u} = \begin{pmatrix} u \\ v \\ w \end{pmatrix} = \begin{pmatrix} R_u\Theta_u Z_u \\ R_v\Theta_v Z_v \\ R_w\Theta_w Z_w \end{pmatrix}. \tag{43}$$

Lamb wave displacements depend on the radial distance, circumferential direction, and frequency et al. It is necessary to investigate the effect of these parameters on the Lamb wave displacement field.

### Characteristics Lamb Wave Displacements in Radial Direction

The displacements of the Lamb wave are governed by the Bessel function in the radial direction. For a large value of $r$, the Bessel functions converge to the asymptotic expression

$$J_s(kr) \to \sqrt{\frac{2}{\pi kr}}\cos\left(kr - \frac{s}{2}\pi - \frac{1}{4}\pi\right) \quad (kr \to \infty). \tag{44}$$

Therefore, the radial components of displacements in the far field satisfy

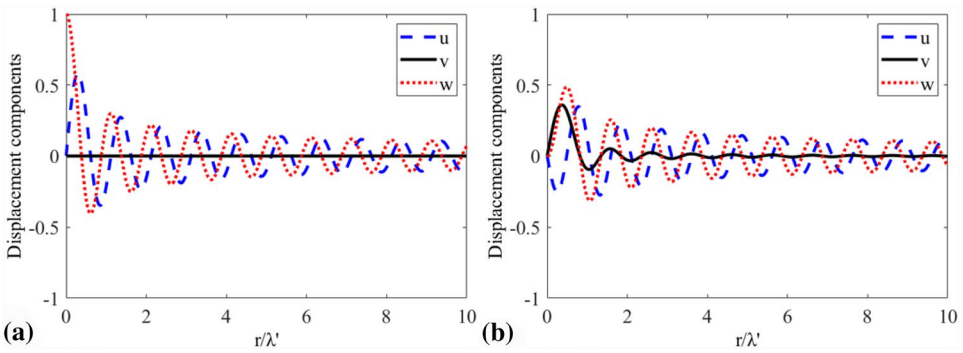


**Fig. 2** Radial components of displacements: **a** $n=0$ and **b** $n=2$

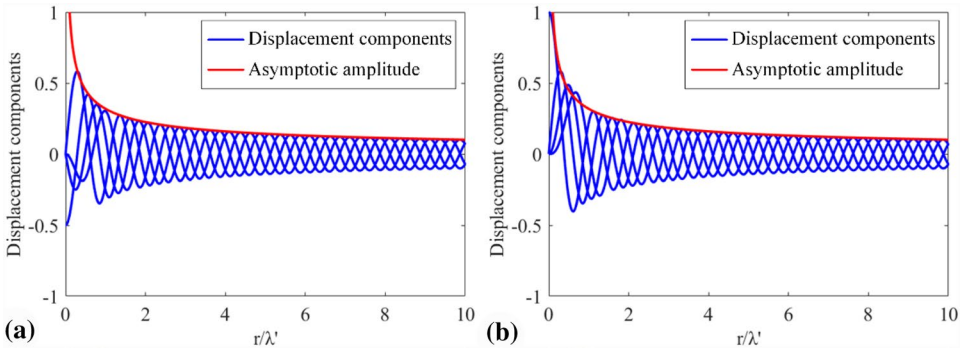


**Fig. 3** Radial component of displacement and asymptotic amplitude: **a** the radial displacement $u$ and **b** the longitudinal displacement $w$

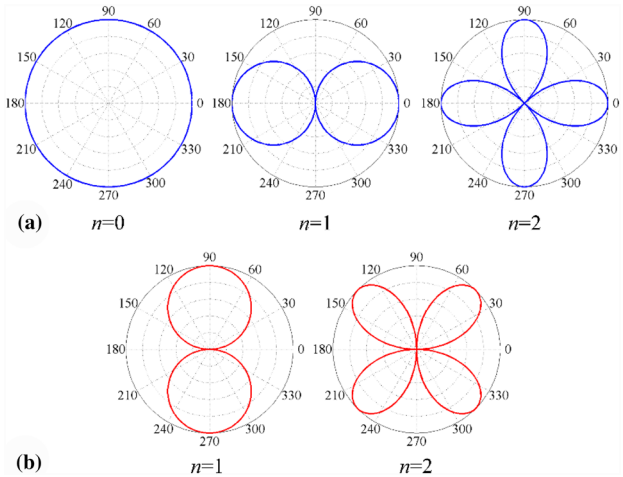


**Fig. 4** Amplitude distributions of displacements in circumferential direction: **a** the radial and longitudinal displacements and **b** the circumferential displacement

Figure 2 presents the radial components of Lamb wave displacements at various propagation distances. The axisymmetric case $n=0$ and a non-axisymmetric case $n=2$ are selected as examples, and $\lambda'$ is the wavelength. As predicted, circumferential displacement vanishes for case $n=0$. For case $n=2$, circumferential displacement exists in the near field and decreases rapidly with the propagation distance increases, which can be neglected after several wavelengths in comparison with the other two displacement components.

Figure 3 presents the radial components of displacement and asymptotic amplitudes. The cases $n=0$–3 are taken into consideration. And the asymptotic amplitude is described as

$$A(kr)=\sqrt{\frac{2}{\pi kr}}, \tag{46}$$

where $k$ is the wave number. In the far field, as expected, asymptotic amplitudes can accurately describe the amplitude decrease. Little discrepancy between the displacement components and the asymptotic amplitudes appears in the near field for the reason that the asymptotic amplitudes of corresponding Bessel functions are precise only in the far field.

$$\begin{cases} R_u^{(m,n)}(r)=\frac{1}{2}\left[J_{n+1}\left(k_m r\right)-J_{n-1}\left(k_m r\right)\right]\to\sqrt{\frac{2}{\pi k_m r}}\sin\left(k_m r-\frac{n}{2}\pi-\frac{1}{4}\pi\right) \\ R_v^{(m,n)}(r)=\frac{1}{2}\left[J_{n+1}\left(k_m r\right)+J_{n-1}\left(k_m r\right)\right]\to 0 \\ R_w^{(m,n)}(r)=J_n\left(k_m r\right)\to\sqrt{\frac{2}{\pi k_m r}}\cos\left(k_m r-\frac{n}{2}\pi-\frac{1}{4}\pi\right) \end{cases} \quad (k_m r\to\infty). \tag{45}$$

In the far field, only radial and longitudinal displacements exist in the Lamb wave. Caused by the sine and cosine functions, the radial and longitudinal displacements have phase differences in the time domain. The asymptotic functions can be divided into two parts, one of which describes the attenuation in amplitude and the other one describes the fluctuation in the time domain. The amplitudes of displacements decrease with the radial distance $r$ following $O(1/\sqrt{r})$ power rule as they propagate away from the origin [36]. Caused by the trigonometric functions contained in asymptotic functions, the displacement patterns become periodic at large radial distances.

## Characteristics of Lamb Wave Displacements in the Circumferential Direction

Lamb wave field versus circumferential component $\theta$ is also concerned for it affects the amplitude distribution in the circumferential direction. Ignoring the effect of the initial phase, the circumferential components of displacement can be expressed as

$$\begin{aligned} \Theta_u^{(m,n)}(\theta)&=\Theta_w^{(m,n)}(\theta)=\mathrm{Re}\left(e^{in\theta}\right)=\cos\left(n\theta\right)=\Theta_1 \\ \Theta_v^{(m,n)}(\theta)&=\mathrm{Re}\left(ie^{in\theta}\right)=-\sin\left(n\theta\right)=\Theta_2. \end{aligned} \tag{47}$$

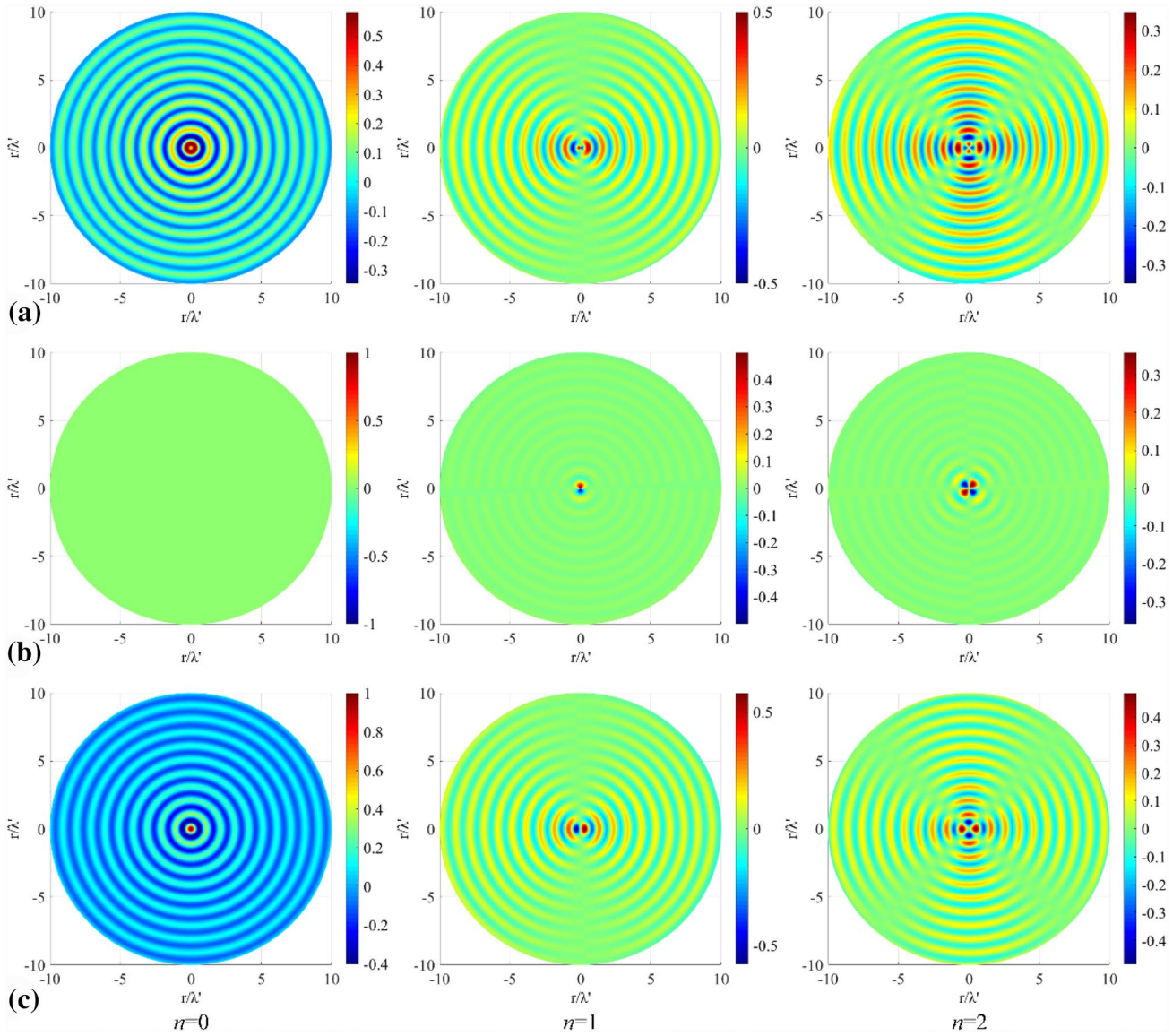


**Fig. 5** Displacement field of Lamb wave: **a** radial displacement $u$ and **b** circumferential displacement $v$ and **c** longitudinal displacement $w$

For the case $n=0$, the amplitude distributions of displacement are uniform in the circumferential direction, representing an axisymmetric wave. For the case, $n\neq 0$, several maxima as well as minima exist in different circumferential directions. The maxima of radial and longitudinal displacements occur at $\theta=N\pi/n$ (integer $N=0, 1, 2, \ldots, 2n-1$), while the maxima of circumferential displacement appear at $\theta=(N+1/2)\pi/n$, as presented in Fig. 4.

## Characteristics of Lamb Wave Displacement Field

Figure 5 presents the amplitude distributions of the across-thickness displacements for Lamb wave at various radial distances and circumferential angles by assuming $Z_u=Z_v=Z_w=1$. As discussed above, only radial and longitudinal displacements exist in the Lamb wave for the case $n=0$. For $n=1$ and $n=2$, circumferential displacements exist near the origin and almost vanish in the far field. There are two and four obvious maxima of amplitude for $n=1$ and $n=2$, respectively. The maxima of radial and longitudinal displacements appear at $\theta=0°$, 180° and $\theta=0°$, 90°, 180°, 270°, while those of circumferential displacement appear at $\theta=90°$, 270° and $\theta=45°$, 135°, 225°, 315°. For each case, the amplitude of displacement decreases with the propagation distance. The results in Fig. 5 show that both propagation distance and propagation direction have effects on the amplitudes of the Lamb wave displacements.

The normalized displacements of A(0,2) mode ($fh=0.75$ MHz-mm) at various propagation directions with different propagation distances are presented in Fig. 6. The

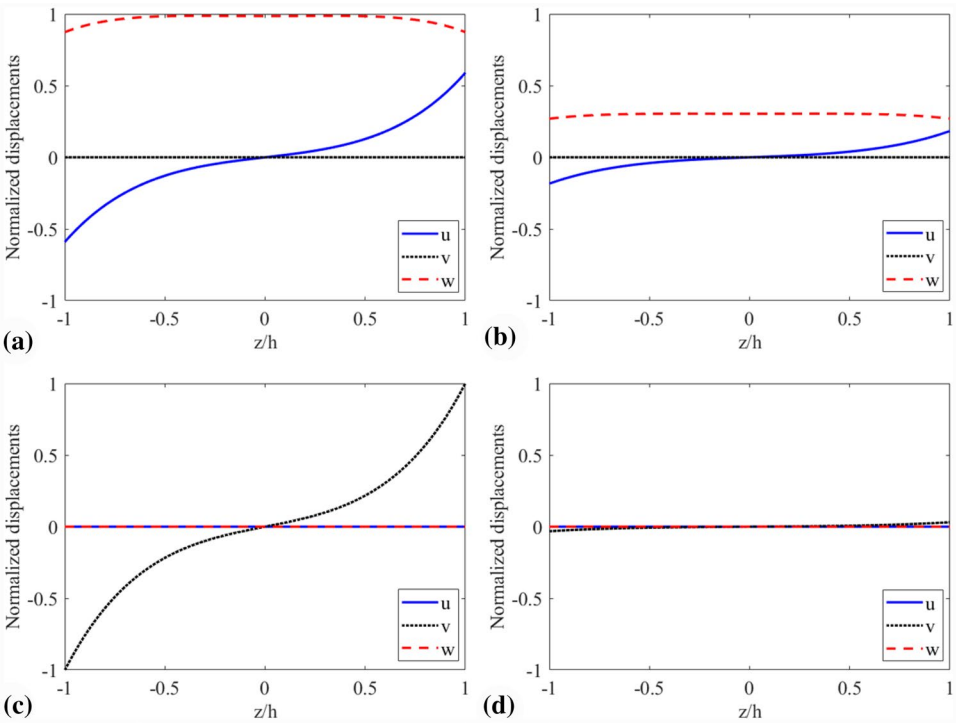


**Fig. 6** Displacements of A(0,2) mode ($fh=0.75$ MHz-mm): **a** $\theta=0°$ and $r=\lambda'$ and **b** $\theta=0°$ and $r=10\lambda'$ and **c** $\theta=45°$ and $r=\lambda'$ and **d** $\theta=45°$ and $r=10\lambda'$

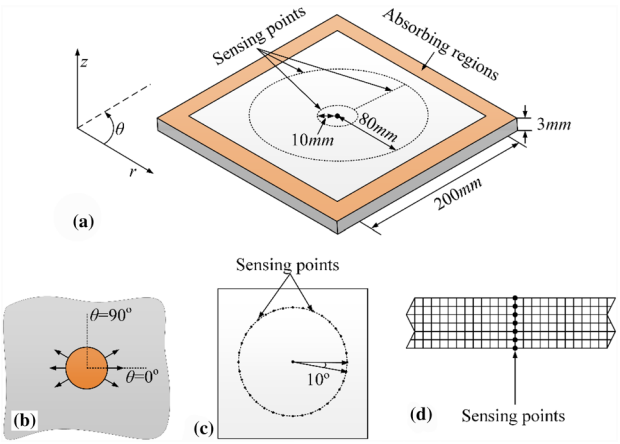


**Fig. 7** Finite element model of aluminum plate: **a** the whole model and **b** the actuator and **c** sensing points at circular and **d** sensing points through thickness

displacements in Fig. 6b, d are normalized by dividing the same coefficients with Fig. 6a, c, respectively. Circumferential displacement vanishes at the direction $\theta=0°$ and exists alone at the direction $\theta=45°$. All of these displacements decrease with the increasing propagation distance, which is caused by the amplitude attenuation of Bessel functions. In the far field, the circumferential displacement can be neglected in comparison with the other two displacements.

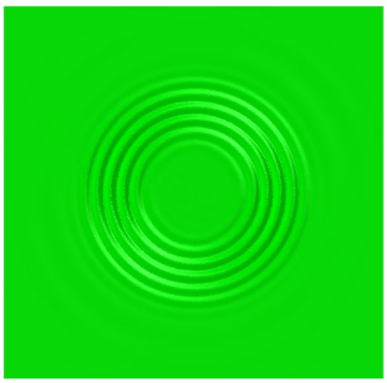

**Fig. 8** Displacement field of circular crested Lamb wave

## Numerical and Experimental Verifications

To verify the theoretical prediction of frequency equations and displacement expressions, both the numerical simulation and experimental study are carried out here.

### Numerical Verification

As presented in Fig. 7a, the simulation is conducted on a $200\times200\times3$ mm plate using ABAQUS. As an example, the aluminum plate is selected. The elasticity modulus, Poisson's ratio and mass density of the aluminum plate are adopted as 70 GPa, 0.33 and 2700 kg/m$^3$. Absorbing

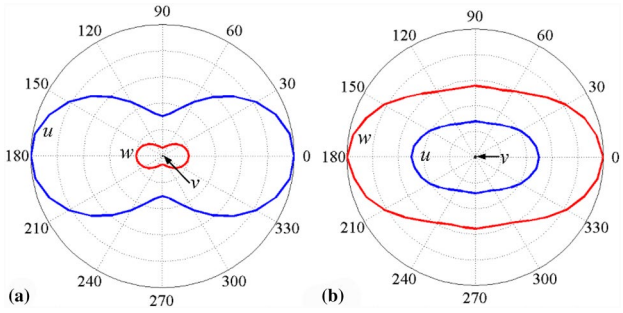


**Fig. 9** Circumferential distributions of Lamb wave displacements: **a** S(0,*) mode after propagating 80 mm and **b** A(0,*) mode after propagating 80 mm

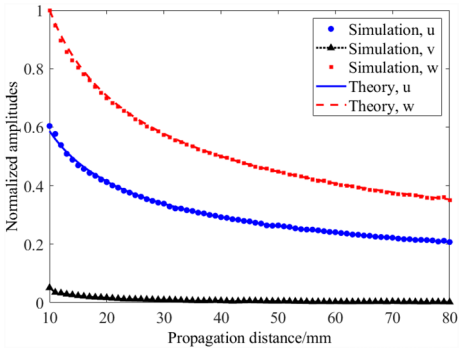


**Fig. 11** Displacement amplitudes of A(0,*) mode varying with propagation distance

regions are added at each edge of the plate [37, 38] to avoid the reflection waves from the edges of the plate. A non-axisymmetric loading is applied at the origin of the upper surface of the plate as an actuator to excite a circular crested Lamb wave, as presented in Fig. 7b. Two sets of sensing points are placed at two circular rings around the origin with the radius 10 mm and 80 mm, respectively. Each set has 36 sensing points with 10° increments shown in Fig. 7c. Moreover, a set of sensing points is placed 80 mm away from the origin through the longitudinal direction to receive the across thickness signals presented in Fig. 7d. To obtain the signal at various propagation distances, a set of sensing points is placed at a straight line through the origin from 10 to 80 mm with a 1 mm increment. A 5-cycle sinusoid tone-burst signal enclosed in a Hanning window with the center frequency $f_c$ at 200 kHz is chosen as an excitation signal. The $N$-cycle sinusoid tone-burst signal $S(t)$ enclosed in the Hanning window with the center frequency $f_c$ can be described as

$$S(t) = \frac{1}{2}\left[1 - \cos\left(\frac{2\pi f_c t}{N}\right)\right]\sin(2\pi f_c t). \tag{48}$$

The mesh density and time step are sufficiently small to resolve the smallest wavelength and simultaneously capture the highest frequency response, respectively.

By applying non-axisymmetric surface loading, both axisymmetric and non-axisymmetric Lamb waves can be excited. At the excitation frequency, only S(0,$n$) and A(0,$n$) can propagate for a long distance. The displacements obtained from sensing points are a linear combination of both axisymmetric and non-axisymmetric modes, denoted as S(0,*) and A(0,*), where

$$\mathrm{S}(0,*) = \sum_{n=0}^{\infty} c_n \mathrm{S}(0,n), \quad \mathrm{A}(0,*) = \sum_{n=0}^{\infty} d_n \mathrm{A}(0,n) \tag{49}$$

and $c_n$ and $d_n$ are coefficients.

The displacement field (longitudinal displacement $w$) of the circular crested Lamb wave is presented in Fig. 8. The Lamb wave displacement field extends as circumferences with the center at the actuator center. At any given moment, Lamb wave at different propagation directions travels for the same distance from the actuator, which is consistent with the theoretical formulations.

Circumferential distributions of the excited Lamb wave displacement are presented in Fig. 9. As predicted, the displacements of both S and A modes are non-axisymmetric which indicates that non-axisymmetric Lamb wave

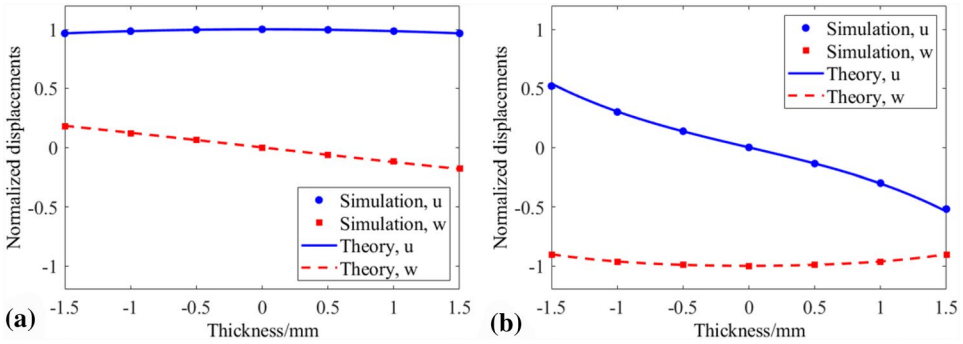


**Fig. 10** Across thickness displacements of Lamb waves excited by non-axisymmetric loading in the far field: **a** S(0,*) mode and **b** A(0,*) mode

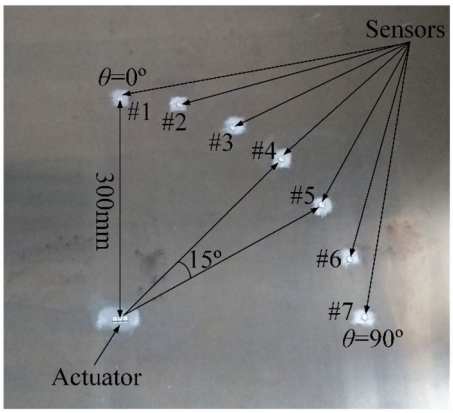


**Fig. 12** Layout and location of actuator and sensors

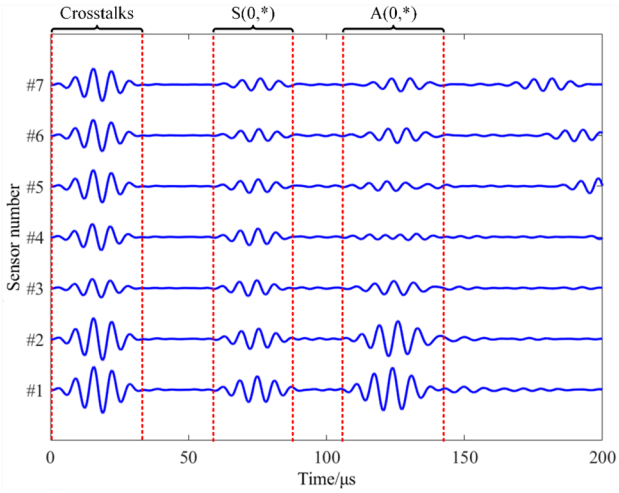


**Fig. 13** Arrival times of S(0,*) mode and A(0,*) mode

exists in plates. The circumferential displacement $v$ can be neglected in comparison with other displacements after propagating 80 mm. This phenomenon is caused by the characteristic of Bessel functions

$$J_{n+1}(kr) + J_{n-1}(kr) \to 0, \quad kr \to \infty \tag{50}$$

Figure 10 shows the across-thickness displacements of Lamb waves after propagating 80 mm. Circumferential displacement is ignored for the amplitude is small enough in comparison to other displacements. The across-thickness displacements obtained from simulations compare very well with theory, providing verification to theoretical formulations.

The displacement amplitudes of A(0,*) mode varying with propagation distance are presented in Fig. 11. As

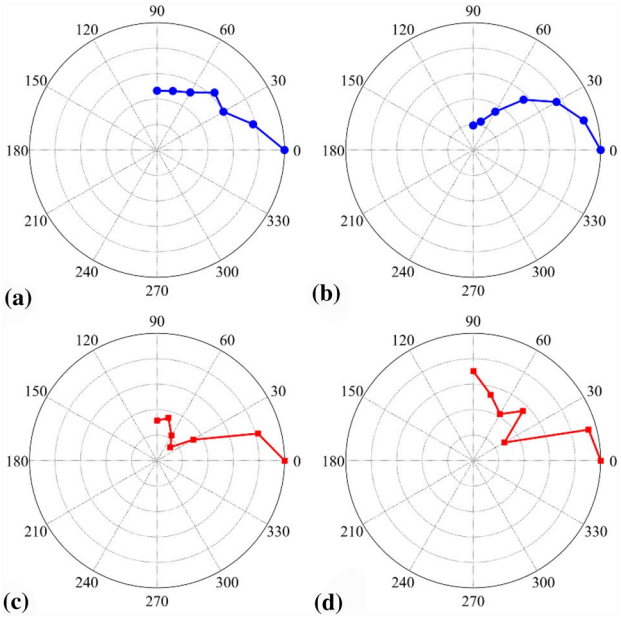


**Fig. 14** Circumferential distributions of the excited Lamb wave modes: **a** S(0,*) mode at 150 kHz and **b** S(0,*) mode at 200 kHz and **c** A(0,*) mode at 150 kHz and **d** A(0,*) mode at 200 kHz

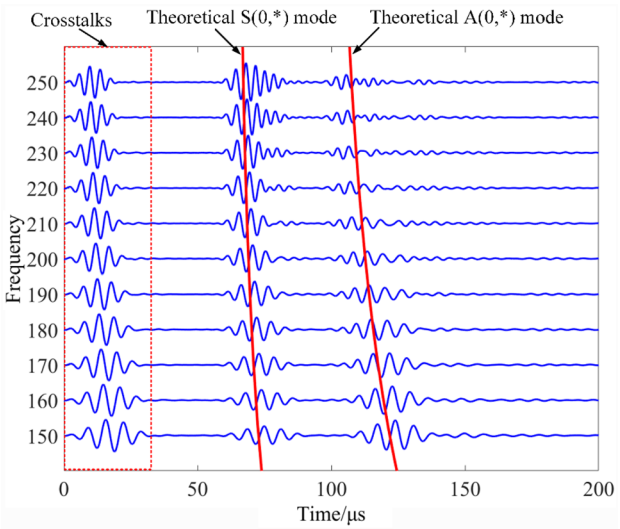


**Fig. 15** Comparison of the arrival time of experiment and theory

predicted in theory, the amplitudes of both radial and longitudinal displacements decrease following $O(1/\sqrt{r})$ in the far field [36] (after propagating 20 mm, the wavelength is about 10 mm) because the amplitude of all modes decreases following the same power rule. Circumferential displacement amplitude rapidly decays to negligible with propagation distance increasing.

## Experimental Verification

The experiment is carried out on a 1250 × 1250 × 3 mm aluminum plate. Three 6 × 6 × 0.5 mm square transducers (American Piezo Ceramics, APC-851) are mounted on the top surface of the plate as an actuator. These thin transducers can reduce the effect of induced bending moment applied to the plate. Seven 8 mm(diameter) × 0.45 mm(thickness) circular transducers (American Piezo Ceramics, APC-851) are placed around the actuators at $\theta = 0°$–$90°$ with 15° increments numbered #1–#7 as sensors. The distance between the actuator and the sensors is 300 mm. The layout and location of the actuator and sensors are presented in Fig. 12. A 5-cycle Hanning window modulated sinusoidal tone burst waveforms with a center frequency at 150–250 kHz with 10 kHz increment is generated as the input signal to each actuator to excite Lamb waves. Signals are generated and received by a damage diagnostic system at a sampling rate of 12 MHz and a sampling point of 8000.

Similar to the simulation, signals obtained from the experiment are also the linear combination of axisymmetric and non-axisymmetric modes as described in Eq. (49). Figure 13 shows the comparison of signals received by different sensors. The blue solid lines represent the Lamb wave signals received by different sensors, and the red dotted lines represent the start and end times of corresponding Lamb modes. The first arrival waveforms in Fig. 13 are cross talks, which are produced by the coupling effect of the circuit. As shown in Fig. 13, the arrival times of both S(0,*) and A(0,*) modes at different propagation directions with the same propagation distance are about the same, which demonstrates that Lamb wave propagates as a circle with the center at the actuator center.

Figure 14 shows the circumferential distributions of the excited Lamb wave. The points represent the amplitudes of signals received by different sensors, and the lines represent the connection lines of points. Both S and A modes have non-uniform distributions at different propagation directions, which proves the existence of non-axisymmetric Lamb wave in plates.

A comparison of the arrival time for circular crested Lamb wave is presented in Fig. 15. The blue lines represent the Lamb wave signals received by sensor #1 at different frequencies in the experiment, and the red lines represent the theoretical arrival times of Lamb modes. The theoretical arrival times of S(0,*) and A(0,*) modes are calculated based on group velocity obtained from frequency equations in Eq. (36). Excellent agreements are observed, which proves the frequency equations of circular crested Lamb wave.

## Conclusions

The complete and exact solutions of circular crested Lamb waves in isotropic plates are obtained and presented with the cylindrical coordinate system. The solutions represent a traveling wave in the radial direction and a standing wave in the other two orthogonal coordinate directions. The displacement field of a circular crested Lamb wave is governed by the Bessel function in the radial direction and harmonic functions in the circumferential direction. Similar to plane Lamb wave, circular crested Lamb wave is divided into two motion types, i.e., S motion and A motion. Two families of circular crested Lamb modes are generated and identified by wavenumber in the radial direction ($k$) and circumferential direction ($n$). Characteristics of circular crested Lamb wave displacements are discussed in detail. Governed by Bessel functions, the radial component describes the amplitude attenuation of displacement. And the circumferential component affects the distribution of amplitude in different propagation directions. Some numerical and experimental results are presented to provide verification for the theoretical formulations. Characteristics of Lamb wave including circular crested wave field, non-axisymmetric property, across thickness displacements and group velocity obtained from simulation and experiment are compared with those of theory. The good agreement between numerical or experimental and theoretical results verifies the theoretical formulations.

**Acknowledgements** In this research work, Dalian Innovation Foundation of Science and Technology (2018J11CY005) and the State Key Laboratory of Structural Analysis for Industrial Equipment (S22303) are gratefully acknowledged.

## Declarations

**Conflict of interest** The authors declare that they have no known competing financial interests or personal relationships that could have appeared to influence the work reported in this paper.

## References

1. Egarguin NJA, Meklachi T, Onofrei D, Harari-Arnold ND (2020) Vibration suppression and defect detection schemes in 1d linear spring-mass systems. J Vib Eng Technol 8(4):489–503
2. Wang Y, Qiu L, Luo Y, Ding R (2021) A stretchable and large-scale guided wave sensor network for aircraft smart skin of structural health monitoring. Struct Health Monit 20(3):861–876
3. Yue N, Khodaei ZS, Aliabadi M (2021) Damage detection in large composite stiffened panels based on a novel SHM building block philosophy. Smart Mater Struct 30(4):045004
4. Cao DY, Zhang YF, Wang YQ (2022) Wave propagation characteristics in submerged pipes conveying viscous flowing fluid based on the shear deformation shell theory. J Vib Eng Technol 10(2):827–839

5. Yang Q, Wang J, Kim S, Chen H, Spencer BF Jr (2022) Design and implementation of a SHM system for a heritage timber building. Smart Struct Syst 29(4):561–576
6. Xin J, Jiang Y, Zhou J, Peng L, Liu S, Tang Q (2022) Bridge deformation prediction based on SHM data using improved VMD and conditional KDE. Eng Struct 261:114285
7. Gonenli C (2022) Effect of cut-out location on the dynamic behaviour of plate frame structures. J Vib Eng Technol 10:1–13
8. Schaal C, Samajder H, Baid H, Mal A (2015) Rayleigh to Lamb wave conversion at a delamination-like crack. J Sound Vib 353:150–163
9. Sherafat MH, Guitel R, Quaegebeur N, Lessard L, Hubert P, Masson P (2016) Guided wave scattering behavior in composite bonded assemblies. Compos Struct 136:696–705
10. Liu Y, Hu N, Deng M, Zhao Y, Li W (2017) Nonlinear Lamb waves in plate/shell structures. Adv Mech 47:201714 (**in Chinese**)
11. Neubeck R, Kexel C, Moll J (2020) Matrix techniques for Lamb-wave damage imaging in metal plates. Smart Mater Struct 29(11):117003
12. Bahador MM, Zaimbashi A, Rahgozar R (2020) Three-stage Lamb-wave-based damage localization algorithm in plate-like structures for structural health monitoring applications. Signal Process 168:107360
13. Chen H, Liu Z, Li Z, Wu B, He C (2020) Application of finite element method in ultrasonic guided waves testing technique. Adv Mech 50:202009 (**in Chinese**)
14. Liu K, Ma S, Wu Z, Zheng Y, Qu X, Wang Y, Wu W (2016) A novel probability-based diagnostic imaging with weight compensation for damage localization using guided waves. Struct Health Monit 15(2):162–173
15. Su Z, Ye L, Lu Y (2006) Guided Lamb waves for identification of damage in composite structures: a review. J Sound Vib 295(3–5):753–780
16. Ochôa P, Infante V, Silva JM, Groves RM (2015) Detection of multiple low-energy impact damage in composite plates using Lamb wave techniques. Compos Part B-Eng 80:291–298
17. Panda RS, Rajagopal P, Balasubramaniam K (2017) Characterization of delamination-type damages in composite laminates using guided wave visualization and air-coupled ultrasound. Struct Health Monit 16(2):142–152
18. Xu H, Cheng L, Su Z, Guyader J-L (2011) Identification of structural damage based on locally perturbed dynamic equilibrium with an application to beam component. J Sound Vib 330(24):5963–5981
19. Rayleigh L (1885) On waves propagated along the plane surface of an elastic solid. Proc Lond Math Soc 1(1):4–11
20. Lamb H (1917) On waves in an elastic plate. Proc R Soc Lond A Math 93(648):114–128
21. Orta AH, Vandendriessche J, Kersemans M, Van Paepegem W, Roozen NB, Van Den Abeele K (2021) Modeling lamb wave propagation in visco-elastic composite plates using a fifth-order plate theory. Ultrasonics 116:106482
22. Kuznetsov S (2020) Lamb waves in anisotropic functionally graded plates: a closed form dispersion solution. J Mech 36(1):1–6
23. Milosavljevic D, Zmindak M, Dekys V, Radakovic A, Cukanovic D (2021) Approximate phase speed of Lamb waves in a composite plate reinforced with strong fibres. J Eng Math 129(1):1–11
24. Thomson WT (1950) Transmission of elastic waves through a stratified solid medium. J Appl Phys 21(2):89–93
25. Saito O, Yu F, Okabe Y (2021) Dispersion relation of Lamb waves in cross-ply composite laminates using multi-layered models. Compos Struct 264:113691
26. Spytek J, Ambrozinski L, Pieczonka L (2022) Evaluation of disbonds in adhesively bonded multilayer plates through local wavenumber estimation. J Sound Vib 520:116624
27. Wang K, Liu M, Cao W, Yang W, Su Z, Cui F (2021) Detection and sizing of disbond in multilayer bonded structure using modally selective guided wave. Struct Health Monit 20(3):904–916
28. Raghavan A, Cesnik CES (2007) 3-D elasticity-based modeling of anisotropic piezocomposite transducers for guided wave structural health monitoring. J Vib Acoust 129:739–751
29. Li L, Faisal Haider M, Mei H, Giurgiutiu V, Xia Y (2020) Theoretical calculation of circular-crested Lamb wave field in single- and multi-layer isotropic plates using the normal mode expansion method. Struct Health Monit 19(2):357–372
30. Haider MF, Giurgiutiu V (2018) Analysis of axis symmetric circular crested elastic wave generated during crack propagation in a plate: a Helmholtz potential technique. Int J Solids Struct 134:130–150
31. Goodman L (1953) Circular crested vibrations of an elastic solid bounded by two parallel planes. University of Illinois, Urbana-Champaign
32. Giurgiutiu V (2007) Structural health monitoring with piezoelectric wafer active sensors. Elsevier, Amsterdam
33. Graff KF (1975) Wave motion in elastic solids. Dover Publications, New York
34. Gazis DC (1959) Three-dimensional investigation of the propagation of waves in hollow circular cylinders. I. Analytical foundation. J Acoust Soc Am 31(5):568–573
35. Rose JL (2014) Ultrasonic guided waves in solid media. Cambridge University Press, Cambridge
36. Huang H, Pamphile T, Derriso M (2008) The effect of actuator bending on Lamb wave displacement fields generated by a piezoelectric patch. Smart Mater Struct 17(5):055012
37. Moreau L, Castaings M (2008) The use of an orthogonality relation for reducing the size of finite element models for 3D guided waves scattering problems. Ultrasonics 48(5):357–366
38. Castaings M, Bacon C, Hosten B, Predoi M (2004) Finite element predictions for the dynamic response of thermo-viscoelastic material structures. J Acoust Soc Am 115(3):1125–1133